A COL17A1 Splice-Altering Mutation Is Prevalent in Inherited Recurrent Corneal Erosions

AMERICAN ACADEMY™ OF OPHTHALMOLOGY

A *COL17A1* Splice-Altering Mutation Is Prevalent in Inherited Recurrent Corneal Erosions

Verity F. Oliver, PhD,[1] *Katherine A. van Bysterveldt, MSc,*[1] *Murray Cadzow, BBioMedSci,*[2] *Bernhard Steger, MD,*[3] *Vito Romano, MD,*[3] *David Markie, PhD,*[4] *Alex W. Hewitt, PhD, FRANZCO,*[5,6] *David A. Mackey, MD, FRANZCO,*[5,6] *Colin E. Willoughby, MD, FRCOphth,*[3,7] *Trevor Sherwin, PhD,*[1] *Philip S. Crosier, PhD,*[8] *Charles N. McGhee, DSc, FRCOphth,*[1,9] *Andrea L. Vincent, MD, FRANZCO*[1,9]

Purpose: Corneal dystrophies are a genetically heterogeneous group of disorders. We previously described a family with an autosomal dominant epithelial recurrent erosion dystrophy (ERED). We aimed to identify the underlying genetic cause of ERED in this family and 3 additional ERED families. We sought to characterize the potential function of the candidate genes using the human and zebrafish cornea.

Design: Case series study of 4 white families with a similar ERED. An experimental study was performed on human and zebrafish tissue to examine the putative biological function of candidate genes.

Participants: Four ERED families, including 28 affected and 17 unaffected individuals.

Methods: HumanLinkage-12 arrays (Illumina, San Diego, CA) were used to genotype 17 family members. Next-generation exome sequencing was performed on an uncle–niece pair. Segregation of potential causative mutations was confirmed using Sanger sequencing. Protein expression was determined using immunohistochemistry in human and zebrafish cornea. Gene expression in zebrafish was assessed using whole-mount in situ hybridization. Morpholino-induced transient gene knockdown was performed in zebrafish embryos.

Main Outcome Measures: Linkage microarray, exome analysis, DNA sequence analysis, immunohistochemistry, in situ hybridization, and morpholino-induced genetic knockdown results.

Results: Linkage microarray analysis identified a candidate region on chromosome chr10:12,576,562–112,763,135, and exploration of exome sequencing data identified 8 putative pathogenic variants in this linkage region. Two variants segregated in 06NZ–TRB1 with ERED: *COL17A1* c.3156C→T and *DNAJC9* c.334G→A. The *COL17A1* c.3156C→T variant segregated in all 4 ERED families. We showed biologically relevant expression of these proteins in human cornea. Both proteins are expressed in the cornea of zebrafish embryos and adults. Zebrafish lacking *Col17a1a* and *Dnajc9* during development show no gross corneal phenotype.

Conclusions: The *COL17A1* c.3156C→T variant is the likely causative mutation in our recurrent corneal erosion families, and its presence in 4 independent families suggests that it is prevalent in ERED. This same *COL17A1* c.3156C→T variant recently was identified in a separate pedigree with ERED. Our study expands the phenotypic spectrum of COL17A1 disease from autosomal recessive epidermolysis bullosa to autosomal dominant ERED and identifies COL17A1 as a key protein in maintaining integrity of the corneal epithelium. *Ophthalmology 2016;123:709-722 © 2016 by the American Academy of Ophthalmology. This is an open access article under the CC BY-NC-ND license (http://creativecommons.org/licenses/by-nc-nd/4.0/).*

Supplemental material is available at www.aaojournal.org.

Technological advances in the clinic and laboratory have allowed us a greater appreciation of the phenotypic and genetic diversity of corneal dystrophies. The International Committee for Classification of Corneal Dystrophies[1,2] has responded to this newfound diversity by developing a clear classification system, considering both clinical features and the underlying genetic cause in its categorical designations. We previously described a 3-generation New Zealand family (06NZ-TRB1) with a unique autosomal dominant corneal dystrophy. Members of the 06NZ-TRB1 family experienced frequent, painful, recurrent corneal erosions from the age of 5 years.[3] The corneal features include small, fine grey anterior stromal flecks, with more unique larger grey-white opacities at the level of the Bowman layer and the immediately subjacent anterior stroma, with increased prominence of the corneal nerves.[3] This corneal appearance is distinct from classic Fleck dystrophy (Online Mendelian Inheritance in Man identifier, 121850), and patients with Fleck dystrophy typically are relatively asymptomatic. Painful recurrent corneal erosions in this family ceased in the patients' second decade, although the resulting accumulation of corneal scarring impaired vision in some

http://dx.doi.org/10.1016/j.ophtha.2015.12.008
ISSN 0161-6420/15

patients. Because the precise genetic change was unknown, the phenotype was assigned as a category 3 under the International Committee for Classification of Corneal Dystrophies classification, which accommodates disease variants in which no genetic locus has been identified (and therefore no known causative gene has been identified, either).[1,4]

Autosomal dominant bilateral corneal dystrophies involving the anterior corneal layers typically are associated with mutations in *TGFBI*[5] or *PIP5K3*.[6] We previously excluded mutations in these and other known corneal dystrophy genes in our family via a combination of microarray technology, direct Sanger sequencing, and linkage analysis.[3] A corneal dystrophy remarkably similar to the one observed in our New Zealand family recently was described as epithelial recurrent erosion dystrophy (ERED; Online Mendelian Inheritance in Man identifier, 122400).[1] Epithelial recurrent erosion dystrophy was described first by Franceschetti and Klein[7] and Franceschetti[8] in a large family. Genetic analysis of its members excluded the candidate corneal dystrophy genes *TGFBI* and *TACSTD2*.[9] Investigations into a similar phenotype in another family (originally described as Thiel-Behnke corneal dystrophy; Online Mendelian Inheritance in Man identifier, 602082)[10–12] linked the candidate genetic loci to chromosome 10q23–24,[12] although no causative mutation was identified.

Next-generation DNA sequencing technology has revolutionized the field of human genetics, allowing single base-pair resolution of DNA variants at the protein-coding (exome) or whole-genome level. Recently, next-generation sequencing facilitated the association of ERED with a missense mutation in *COL17A1* (Online Mendelian Inheritance in Man identifier, 113811).[13] In this article, we describe the identification of a heterozygous *COL17A1* c.3156C→T mutation in the 06NZ-TRB1 ERED family via single nucleotide polymorphism microarray linkage analysis and next-generation exome sequencing. Segregation of the c.3156C→T *COL17A1* mutation, which is predicted to be splice altering, was confirmed in additional 06NZ-TRB1 family members, as well as in 3 families located elsewhere in New Zealand, Tasmania, and the United Kingdom. We also identified a cosegregating, nonsynonymous variant in the *DNAJC9* gene in our NZ06-TRB1 family that may modify disease presentation in these individuals. Finally, we confirmed functionally relevant expression of *COL17A1* and *DNAJC9* in both the human and zebrafish cornea.

Methods

Collection of DNA Samples

This study adhered to the principles of the Declaration of Helsinki and received institutional ethics approval (Northern A Health and Disability Ethics Committee, NTX/06/12/161; Northern Ireland Office for Research Ethics Committee, 350/03). After obtaining informed consent, genomic DNA was extracted from peripheral venous blood or saliva as described previously.[3] Samples were collected from 17 members of the 06NZ-TRB1 family (7 affected and 10 unaffected members) and from 4 members of the 15NZ-LED1 family (3 affected members and 1 member with unknown status). Samples from the additional families were received as genomic DNA from Tasmania (11 affected and 4 unaffected members) and the United Kingdom (7 affected and 2 unaffected members).

Clinical Examination of Patients

All family members underwent a comprehensive clinical examination to determine the presence or absence of disease (described previously[3]). This included visual acuity, slit-lamp examination, intraocular pressure (Goldmann applanation tonometry), and, in selected affected individuals, clinical photography and in vivo confocal microscopy (IVCM) with the Heidelberg Retina Tomograph 2 Rostock Cornea Module (Heidelberg Engineering GMBH, Heidelberg, Germany).[3,14] Representative IVCM images from all corneal layers were selected for the United Kingdom family (UKOGA) by 2 experienced examiners (B.S., V.R.) for analysis of pathologic changes. A validated IVCM grading scale for the quantification of anterior corneal stromal haze and fibrosis was applied.[15]

Linkage Analysis Using HumanLinkage-12 Arrays

HumanLinkage-12 arrays (Illumina, San Diego, CA) were used to genotype 17 06NZ-TRB1 family members (7 affected and 8 unaffected members and 2 members with unknown status subsequently confirmed as unaffected). Genotypes were imported into ALOHOMORA[16] for subsequent manipulation. Mendelian errors were identified with PedCheck,[17] and unlikely close-recombinant genotypes were identified with Merlin[18] and were removed before multipoint parametric linkage analysis with Allegro version 2[19] using the deCODE genetic map.[20]

Screening of Candidate Genes

Protein–protein interactions were analyzed with Search Tool for the Retrieval of Interacting Genes/Proteins (STRING).[21] This created functional protein association networks among known corneal dystrophy genes located within the reduced interval of the linkage region, identifying 8 genes of interest. Primer pairs for amplicons spanning at least 1 full exon, and its 5′ and 3′ intron–exon boundaries, were designed with the National Center for Biotechnology Information's Primer-BLAST (available at www.ncbi.nlm.nih.gov/tools/primer-blast/) for all coding exons within the identified genes of interest, as shown in Supplemental Table 1 (available at www.aaojournal.org). Sanger sequencing was performed on an ABI 3700 sequencer (Applied Biosystems, Waltham, MA) as previously described.[3,22] Sequence chromatograms were compared with reference sequences in CodonCode Aligner version 4.2.3 (CodonCode Corporation, Centerville, MA).

Exome Sequencing and Bioinformatic Analysis

DNA from 2 affected individuals (II.5 and III.3, an uncle–niece pair; Fig 1A) was sent to the Otago Genomics Facility (New Zealand Genomics Ltd.) for library preparation, exome enrichment, and Illumina HiSeq sequencing (Illumina, Inc., San Diego, CA). Illumina TruSeq DNA sequencing libraries and TruSeq 64Mb exome enrichment were carried out according to the manufacturer's instructions. Exomes were subjected to 100-bp paired-end sequencing using the Illumina HiSeq2000 instrument.

Reads were aligned to the human reference GRCh37 with Burrows-Wheeler Alignment tool (BWA).[23] Aligned reads then were marked for duplicates with Picard,[24] and base quality score recalibration and realignment of local insertions and deletions

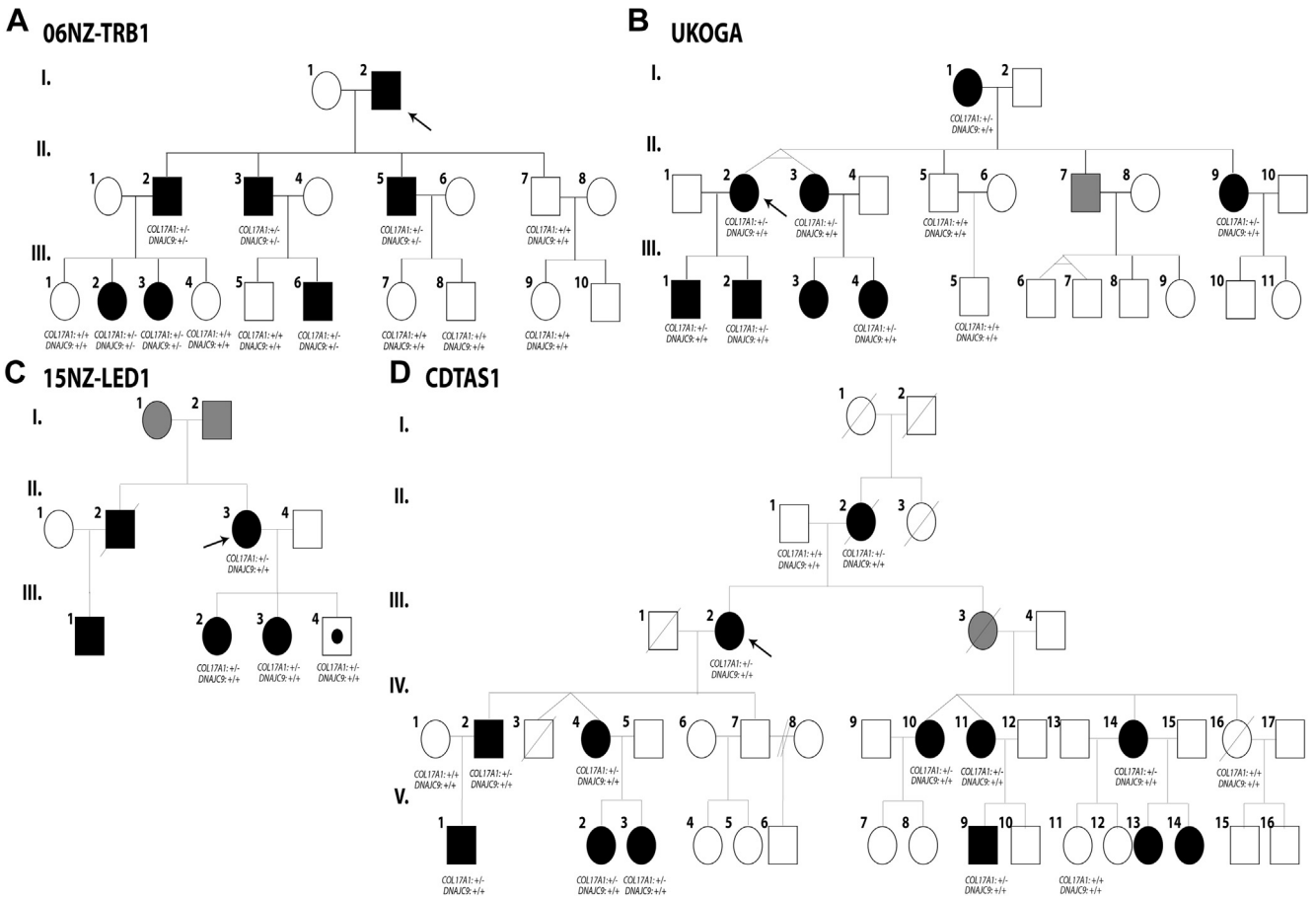

Figure 1. Pedigrees of 4 families with phenotypically similar epithelial recurrent erosion dystrophy and segregation of the identified COL17A1 and DNAJC9 variants. **A**, 06NZ-TRB1 family from New Zealand.[3] **B**, UKOGA family from the United Kingdom. **C**, 15NZ-LED1 family from New Zealand. **D**, CDTAS1 family from Tasmania, Australia. Males are represented as squares, and females are represented as circles. Unaffected family members are shaded white, affected family members are shaded black, unknown status members are shaded grey, and a presumed affected family member (based on genetic analysis) is shaded white with a black center. The probands in each family are indicated by an arrow.

were performed with the Genome Analysis Toolkit.[25] Recalibrated reads were genotyped with the Genome Analysis Toolkit unified genotyper,[26] and variant quality scores were readjusted to standard hard filtering parameters.

Variants were annotated with SnpEff to identify genes, locations within genes, and possible impact on genes,[27] and then were filtered by the critical region (as defined by linkage), by heterozygosity in both affected family members, and finally by population allele frequency in ESP6500[28] and the 1000 Genomes data sets.[29] MutationTaster,[30] MutationTaster2,[31] and Human Splicing Factor[32] were used to predict the effect of variants on splicing. MutationTaster[30,31] and PolyPhen-2[33] were used to predict pathogenicity of missense variants.

Sanger Sequencing Confirmation

Primer pairs flanking the variants of interest were designed with Primer3Plus (available at: primer3plus.com/) and the National Center for Biotechnology Information's BLAST (Basic Local Alignment Search Tool; www.ncbi.nlm.nih.gov/BLAST). Primers for *COL17A1* c.3156C→T were 5′-CGTGGGGAGAACATGTCC-3′ (forward) and 5′-AAAGTCTCGCCTGTGATGGT-3′ (reverse) and those for *DNAJC9* c. 334 G→A were F: 5′-CCCTTCCCTGGTCCCTAGTT-3′ (forward) and 5′-CTTGATGAACTGGTATGCCCA-3′ (reverse). Polymerase chain reaction (PCR) analysis was performed using the AmpliTaq Gold DNA polymerase (Life Technologies, Waltham, MA), with a final $MgCl_2$ concentration of 1.5 mmol/L. Polymerase chain reaction amplicons were purified using the DNA Clean & Concentrator-5 PCR Purification Kit (Zymo Research, Irvine, CA) according to the manufacturer's instructions. Sanger sequencing was performed on an ABI 3700 sequencer as described previously.[3,22] Sequence data were compared with the National Center for Biotechnology Information reference sequence NM_000494.3 with CodonCode Aligner Software version 4.2.3 (CodonCode Corporation).

Microsatellite Marker Analysis

Microsatellite markers were identified adjacent to *COL17A1* with the UCSC Genome Browser microsatellite track. Microsatellite repeats were identified within *COL17A1* (19×CA repeat; chr10:105815203−105815240, GRCh37) and *OBFC1* (20×AT repeat; chr10:105674094−105674133), as shown in Supplemental Figure 1 (available at www.aaojournal.org). Primers were designed with Primer3Plus. Primers for *COL17A1* (19×CA) were 5′-HEX-CCAAGACTGTGGTCCCACTT-3′ (forward) and 5′-ACTCACTTCCAACTGCAGGA-3′ (reverse; 60° C annealing temperature). Primers for *OBFC1* (20×AT) were 5′-FAM-TGATTGTACCACTGCCTTCCA-3′ (forward) and 5′-TCCACA

ACCACAGCAAGACA-3′ (reverse; 63° C annealing temperature). Polymerase chain reaction was performed on 250 ng DNA in a 50-μl reaction with AmpliTaq Gold DNA Polymerase (Life Technologies) according to the manufacturer's guidelines. Polymerase chain reaction products were cleaned with the DNA Clean & Concentrator-5 PCR Purification Kit (Zymo Research) according to the manufacturer's instructions. The purified samples were run alongside a 500 LIZ Size Standard (Applied Biosystems) on an ABI 3730 capillary sequencer (Applied Biosystems). The microsatellite results were allele binned with the STRand analysis freeware (available at: www.vgl.ucdavis.edu/STRand).

Immunohistochemistry

Immunohistochemistry was performed to show expression of COL17A1 and DNAJC9 in both human and zebrafish cornea. Cryosections of 16 to 20 μm were prepared from fresh keratoconic human corneal buttons (collected during corneal transplant surgeries; New Zealand Eye Bank, www.eyebank.org.nz/) and 4% paraformaldehyde−treated zebrafish tissue (isolated adult eyes and whole embryos) as follows. Tissues were processed though a sucrose gradient, embedded in a 2:1 25% sucrose−O.C.T. compound media (Tissue-Tek; Sakura Finetek U.S.A., Inc., Torrance, CA) and snap-frozen on dry ice, then stored at −80° C until use. Cryosections were mounted on Superfrost Plus Microscope Slides (Fisher Scientific, Hampton, NH) and dried overnight. For immunohistochemistry, sections were rehydrated in 0.1 M phosphate-buffered saline (PBS), then digested with 2 mg/ml testicular hyaluronidase for 1 hour at 37° C. Sections were permeabilized in −20° C methanol for 20 minutes, washed with 0.1 M PBS, and treated in 20 mmol/L glycine for 30 minutes. Sections then were blocked with 2% normal goat serum in PBS (plus 0.1% Triton X-100) for 30 minutes at room temperature before labelling. A mouse monoclonal antibody raised against the NC16a-domain of human COL17A1 (catalog no. ab79878; Abcam, Cambridge, UK) was used at a dilution of 1:40 for both species. For DNAJC9, a rabbit monoclonal antibody raised against a synthetic peptide corresponding to residues in human DNAJC9 (catalog no. EPR9856; Abcam) was used at a dilution of 1:100 for both species. A polyclonal rabbit antimouse laminin (laminin, α 1) primary antibody (catalog no. L-9393; Sigma-Aldrich, St. Louis, MO) was used at 1:60 (8.3 ng/μl) to label the basement membrane.[34] The primary antibody was incubated overnight at 4° C in a humidifying chamber. Sections were washed with 0.1 M PBS before secondary antibody application. For COL17A1 detection, goat antimouse immunoglobulin G Alexa-546 (catalog no. A11003; Molecular Probes, Eugene, OR) at 1:1000 for human tissue and 1:400 for zebrafish tissue were used. Goat antirabbit immunoglobulin G Alexa-488 (catalog no. A11031; Life Technologies) was used at 1:300 (6.7 ng/μl) for laminin and DNAJC9 detection in both human and zebrafish tissue. Secondary antibody labelling was performed for 2 hours at room temperature in the dark to prevent quenching of the conjugated fluorophores. Unbound secondary antibody was removed by washing sections with 0.1 M PBS. Sections then were stained with 4′,6-diamidino-2-phenylindole to show cell nuclei and were mounted in Citiflour Antifadent-mounted media (Citifluor Ltd, London, UK). Labelling was visualized using confocal microscopy.

Zebrafish Whole-Mount In Situ Hybridization

Zebrafish were used with institutional ethics approval from the University of Auckland Animal Ethics Committee (reference no. 001343). Hybridization of antisense RNA probes specific to a transcript of interest were used to visualize expression via antibody-conjugated alkaline phosphatase staining.[35] Digoxigenin (Roche, Penzberg, Germany)−labelled antisense RNA probes were produced against zebrafish orthologs of *COL17A1* (*Col17a1a* and *Col17a1b*, as previously published[36]) and *Dnacj9* (Ensembl transcript ENSDART00000137643, drDNAJC9_WISH_F2: AGAAGCTCCAGACTCGGAGA and drDNAJC9_WISH_R2: GCCCATCTCCTCCTGCATTT). Reverse-transcriptase PCR was performed on cDNA from embryos 8 days after fertilization to amplify the region of interest. The PCR products then were ligated into the pCR II-TOPO vector (Life Technologies), linearized with SpeI, NotI, or BamHI (NEB; New England Biolabs, Ipswich, MA), and transcribed with T7 or Sp6 polymerase. Embryos were prepared by fixation in 4% paraformaldehyde (ProSciTech, Thuringowa Central, Australia) overnight and stored in 100% methanol. An established whole-mount in situ hybridization protocol was followed as previously described.[35] Posthybridization staining was performed using an alkaline phosphatase−conjugated anti-digoxigenin (DIG) antibody. Samples were imaged under a Leica MZ16FA stereomicroscope with a Leica DC490 camera and software (Leica, Wetzlar, Germany).

Morpholino Microinjections

Morpholinos were designed and synthesized by GeneTools LLC (Philomath, OR): Col17a1a_TB:TGGTTGTTGTTAGCTTGTCCATTCC to target NM_001145565.1 and DNAJC9_SB_Disease:GTAATCTGCGGCAGAAGTGTCACAA to target exon 2 of ENSDART00000044150. The Standard Control Morpholino from GeneTools LLC was used as a control. Morpholinos were resuspended to 5-mmol/L stock solutions, from which 0.25-mmol/L (*Col17a1a*) and 0.5-mmol/L (*Dnajc9* and control) injection mixes were made, including 2X Phenol Red dye. One nanoliter of morpholino was injected into single-cell embryos. Embryos were grown in the dark at 28° C and examined using a Zeiss Discover V20 stereo microscope and camera (Zeiss, Oberkochen, Germany).

Results

Phenotype Description

Four white families with suspected autosomal dominant ERED were identified independently (Fig 1). These families are not knowingly related to each other, nor to an ERED family previously described in New Zealand.[37] The phenotype of the index New Zealand family (06NZ-TRB1; Fig 1A), as previously described,[3] was remarkably similar to the other 3 families (Table 1). In all families, affected individuals presented between 5 and 7 years of age for recurrent significant corneal epithelial erosions. As the individuals aged, these episodes tended to decrease in frequency and eventually burnt out, variably from the third to fourth decade. Symptoms continuing beyond the cessation of erosions predominantly were foreign body sensation, photophobia, and a variable reduction in vision.

All families had features on slit-lamp biomicroscopy similar to those described in the index family, additional examples of which are shown in Supplemental Figure 2 (available at www.aaojournal.org).[3] The key features of this 06NZ-TRB1 New Zealand corneal phenotype are a small number of focal, disc-shaped, circular, or wreath-like grey-white opacities (typically 0.2−1.5 mm in diameter) involving the Bowman layer and adjacent anterior stroma on a relatively subtle background of numerous smaller (<100 μm) grey flecks limited to the anterior 20% of the stroma (Fig 2). The earliest lesions are similar in general appearance to the minor Bowman layer scarring that follows small, superficial corneal foreign bodies. Symptoms of recurrent corneal erosions typically commence at approximately

Table 1. Clinical Features of the 4 Epithelial Recurrent Erosion Dystrophy Families: 06NZ-TRB1, UKOGA, 15NZ-LED1, and CDTAS1

Family Identification	Patient Identification	Affected Status	Genotype		Sex	Age (yrs)			Visual Acuity		Corneal Findings	
			COL17A1	*DNAJC9*		*At Last Examination*	*At Onset*	*At Offset*	*Right Eye*	*Left Eye*	*Right Eye*	*Left Eye*
06NZ-TRB1	I.2	Affected	—	—	M	64	"Childhood"	?	6/7.5−1	6/7.5−	[3]Vincent et al	[3]Vincent et al
	II.2	Affected	C/T	G/A	M	41	10	21	6/12	6/7.5	[3]Vincent et al	[3]Vincent et al
	II.3	Affected	C/T	G/A	M	39	6	13	6/6+	6/6	[3]Vincent et al	[3]Vincent et al
	II.5	Affected	C/T	G/A	M	38	5	22	6/6	6/6+1	[3]Vincent et al	[3]Vincent et al
	III.2	Affected	C/T	G/A	F	14	5	Continuing	6/5	6/5	[3]Vincent et al	[3]Vincent et al
	III.3	Affected	C/T	G/A	F	12	5	Continuing	6/5	6/5−1	[3]Vincent et al	[3]Vincent et al
	III.6	Affected	C/T	G/A	M	10	5	—	6/6	6/6	[3]Vincent et al	[3]Vincent et al
UKOGA	I.1	Affected	C/T	G/G	F	75	7	?	6/9	6/12	3−4 Minor attacks per year in both eyes	
	II.2	Affected	C/T	G/G	F	42	7	Continuing	6/9	6/5	PTK 1997 in both eyes	
	II.3	Affected	C/T	G/G	F	55	7	Continuing	6/6	6/9	PTK 2011 in both eyes reduced frequency and severity	
	II.7	Putative affected	—	—	M	30	? (4−6)		6/12	6/5	Almost MDF pattern in central area at mild superficial stromal granularity; prominent corneal nerves	Mild discrete granularity in superficial stroma; 2 wreath-like lesions
	II.9	Affected	C/T	G/G	F	37	6	35 (After excimer)	6/4	6/4	PTK 2006/2010	
	III.1	Affected	C/T	G/G	M	25	7	Continuing	6/5	6/5	2 Attacks per year	
	III.2	Affected	C/T	G/G	M	21	7	Continuing	6/4	6/4	One attack per 18 months	
	III.3	Affected	—	—	F	10	10	Continuing	—	—	—	—
	III.4	Affected	C/T	G/G	F	17	6−7	13	6/6	6/9		Scar after BCL-related microbial keratitis
15NZ-LED1	II.2	Affected	—	—	M	—	—	—	—	—	—	—
	II.3	Affected	C/T	G/G	F	30	? (<8)	?	—	—	Faint stromal scar and healing epithelial defect	
	III.1	Affected	—	—	M	—	—	—	—	—	—	—
	III.2	Affected	C/T	G/G	F	10	8.3	Continuing	6/6+1	6/18ph	Both eyes L>R, clear corneas nil noted on examination	
	III.3	Affected	C/T	G/G	F	9	8.5	Continuing	6/6	6/6		Subepithelial cysts/ vacuoles (mild)
	III.4	Predicted affected	C/T	G/G	M	—	—	—	—	—	—	—
CDTAS1	II.2	Affected	C/T	G/G	F	—	—	—	—	—	—	—
	III.2	Affected	C/T	G/G	F	61	30	—	HM	6/12	Marked opacification	Anterior stromal haze
	IV.2	Affected	C/T	G/G	M	41	5	—	6/6	6/9	Stromal scarring and anterior stromal haze	Stromal scarring and anterior stromal haze
	IV.4	Affected	C/T	G/G	F	40	28	—	6/9	6/9	Mild anterior stromal haze	Mild anterior stromal haze
	IV.10	Affected	C/T	G/G	F	—	—	—	—	—	—	—
	IV.11	Affected	C/T	G/G	F	44	6	—	6/5	6/5	Mild anterior stromal haze	Mild anterior stromal haze
	IV.14	Affected	C/T	G/G	F	42	6	—	6/5	6/6	Both eyes anterior stromal haze; prominent nerves	
	V.1	Affected	C/T	G/G	M	4	12	—	6/5	6/9	Anterior stromal haze	Anterior stromal haze
	V.2	Affected	C/T	G/G	F	7	19	—	6/4	6/5	Mild anterior stromal haze	Mild anterior stromal haze
	V.3	Affected	C/T	G/G	F	6	16	—	6/9	6/9	Mild anterior stromal haze	Mild anterior stromal haze
	V.9	Affected	C/T	G/G	M	5	18	—	6/5	6/4	Anterior stromal haze	Anterior stromal haze
	V.13	Affected	—	—	F	6	12	—	6/4	6/6	Clear	Clear
	V.14	Affected	—	—	F	6	9	—	6/5	6/5	Anterior stromal haze	Anterior stromal haze

BCL = B-cell lymphoma; F = female; L = left; M = male; MDF = map-dot-fingerprint dystrophy; ph = pinhole; PTK = protein tyrosine kinase; R = right; — = no information available; ? = unsure.

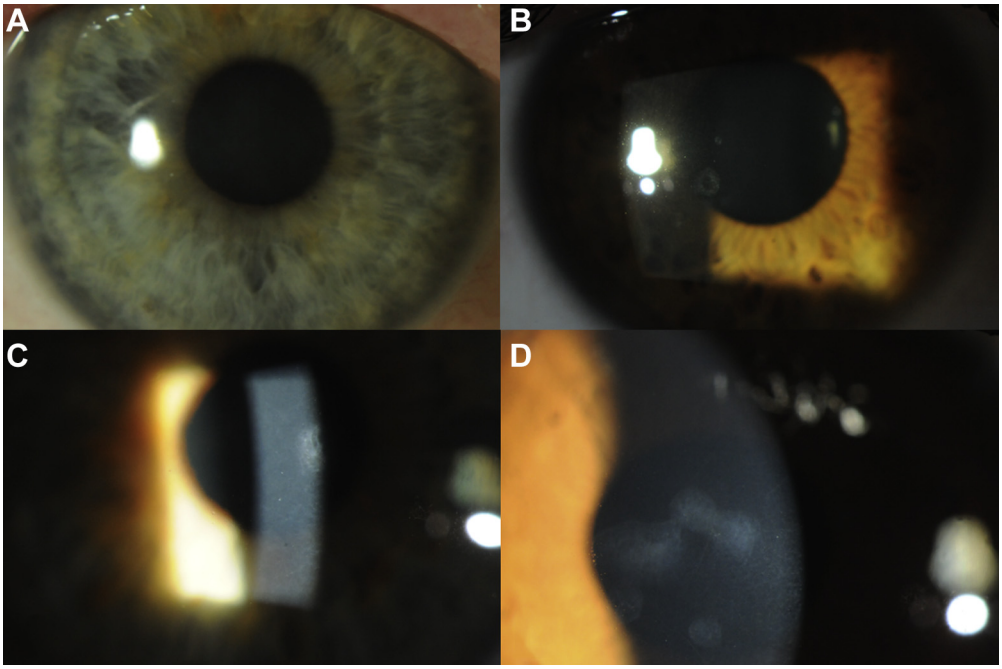

Figure 2. Slit-lamp photographs showing the clinical phenotype observed in the UKOGA family. **A**, Individual I.1 showing generalized superficial stromal haze shown as a grayish haze across the pupillary zone. **B**, Individual II.9 showing discrete, grayish, white oval-round or wreath-like opacities with distinct margins at the level of the Bowman layer or superficial stroma. **C**, Individual II.3 showing small discrete flecks in the superficial stroma with a larger round opacity and superficial stromal haze. **D**, Individual III.4 showing round and wreath-like opacities with distinct margins at the level of the Bowman layer or superficial stroma with small discrete flecks in the superficial stroma.

6 years of age and seem to precede these corneal clinical signs. Although there was a tendency for stromal opacities to appear and gradually increase throughout life, variable expression was present within family members. The phenotypic variability observed in the United Kingdom family in 4 individuals spanning 3 generations is demonstrated in Figure 2.

In vivo confocal microscopy examination in the UKOGA family showed features similar to those in the index 06NZ-TRB1 New Zealand family: brightly hyperreflective polymorphous intraepithelial opacities were present in the epithelium, although invisible on biomicroscopic examination (Fig 3A). Areas with clinically visible disc-like opacities showed bowl-like epithelial thickening extending into the anterior stroma, with complete destruction of Bowman layer and the subepithelial nerve plexus (Fig 3B). The adjacent anterior stroma was remarkable for diffuse accumulation of anterior stromal extracellular matrix (grade 2; Fig 3C). Although anterior stromal extracellular matrix accumulation was limited to focal clinical lesions in younger patients, it was not limited to these lesions in older individuals (Fig 3D). Also, the corneal stroma in younger patients did not yield any abnormal findings, whereas patients older than 60 years were found to show needle-like stromal opacities affecting the anterior more than the posterior stroma (Fig 3E), resembling findings previously described in granular and Reis-Bücklers corneal dystropy.[15,38] The corneal endothelium was not affected. Only single endothelial guttae were found in 1 female patient who was 74 years of age (Fig 3F).

Single Nucleotide Polymorphism Arrays Identify a Linkage Region

Genome-wide analysis of haplotypes conserved between 7 affected 06NZ-TRB1 family members identified a single peak on chromosome 10 reaching the maximum logarithm of the odds score of 2.7, as depicted in Supplemental Figure 3 (available at www.aaojournal.org). The linkage region corresponded to haplotypes between single nucleotide polymorphisms rs1111060 and rs11195400 (specifically, chr10:12,576,562−112,763,135, GRCh37) and covered 100.14 Mb, as shown in Supplemental Figure 4 (green haplotype; available at www.aaojournal.org). All 7 affected 06NZ-TRB1 individuals we examined carried this haplotype. Two individuals of unknown status (too young to have demonstrated disease) did not carry this haplotype and, by 10 years of age, did not demonstrate recurrent erosions. These individuals retrospectively had their status reassigned to unaffected, bringing the maximum logarithm of the odds score to 3.3.

Candidate Gene Screen in 06NZ-TRB1

The 100-Mb linkage region identified on chr10:12,576,562−112,763,135 contains approximately 996 genes. To identify candidate disease-causing genes, we created functional protein association networks between known corneal genes and those within our chr10:12,576,562−112,763,135 linkage region.[21] This identified 8 strong candidate genes of interest that are located within the reduced interval, expressed in the cornea, make biological sense, and interact with other known corneal proteins, as shown in Supplemental Table 2 (available at www.aaojournal.org). Sanger sequencing of all coding exons of these 8 candidate genes was performed on 2 brothers discordant for disease from the 06NZ-TRB1 family. No sequence variants were found in the genomic DNA sequences examined between these 2 individuals.

Exome Sequencing Results in 06NZ-TRB1

Given the size of the linkage region and the number of genes it contained, exome sequencing was performed on 2 affected individuals (Fig 1A, II.5 and III.3, an uncle−niece pair). Bioinformatic filtering identified 46 heterozygous variants with

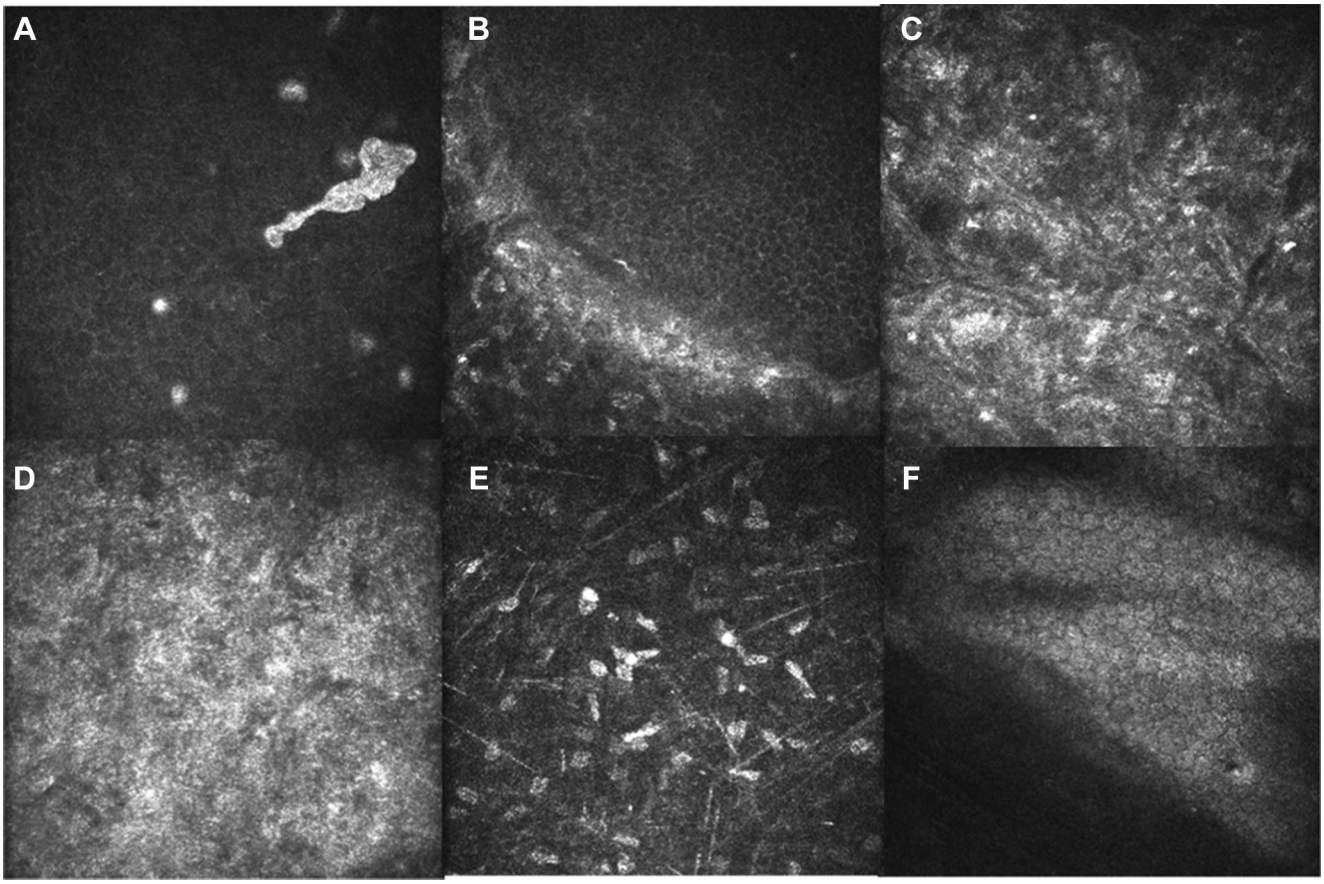

Figure 3. In vivo confocal microscopy images throughout the cornea of affected UKOGA family members: (**A**) epithelium in II.9, (**B**) epithelium stromal interface in III.4, (**C**) anterior stroma in III.4, (**D**) anterior stroma in I.1, (**E**) stroma in II.9, and (**F**) endothelium in I.1.

allele frequencies of less than 0.001 in the National Heart, Lung, and Blood Institute ESP Exome Variant Server and 1000 Genomes databases,[28,29] as shown in Supplemental Table 3 (available at www.aaojournal.org).[39] MutationTaster was used to predict pathogenicity of all heterozygous variants, as provided in Supplemental Table 3 (available at www.aaojournal.org).[30,31] The evidence supporting 4 of the variants was poor because of low read depth; therefore, these variants were given a low priority and were not investigated further. Of the remaining 42 variants, 10 were homozygous in more than 4 individuals and a further 8 were heterozygous in more than 20 individuals in the 1000 Genomes Project data.[39] In total, we identified 8 potential disease-causing variants in our whole-genome exome sequencing data, as shown in Table 2 and Supplemental Table 4 (available at www.aaojournal.org).

Previously, Sullivan et al[40] identified an ERED phenotype–associated linkage region between markers D10S677 (chr10:95,964,310) and D10S1671 (chr10:106,852,499) in a family originally described as having Thiel-Behnke corneal dystrophy.[12] Four of our potential disease-causing variants lie in genes found within this region: *ARHGAP19*, *COL17A1*, *GBF1*, and *SLIT1*. *COL17A1* previously was excluded as the causative gene in this previously described corneal dystrophy family.[40] However, the *COL17A1* variant c.3156C→T, which superficially seems to produce a synonymous substitution in codon 1052 encoding glycine (chr10:105,797,446, GRCh37; ENST00000353479; NM_000494), segregated with disease in our original New Zealand family (06NZ-TRB1; 7 affected and 10 unaffected individuals), as confirmed by Sanger sequencing (Fig 1; Table 1). This variant is present only once in the Exome Aggregation Consortium database (available at exac.broadinsititute.org/), with an allele frequency of 8.249e-06.[41] Jonsson et al[13] predicted (using a minigene splicing assay and in vitro mutagenesis) that the c.3156C→T variant leads to the introduction of a splice donor site and causes truncation of exon 46, resulting in the hypothesized insertion of 1 amino acid and deletion of 17 amino acids; (p.Gly1052_Thr1070delinsAla).

The only in silico–predicted missense variant detected by whole-exome sequencing was in *DNAJC9* (c.334G→A, p.D112N, chr10:75,005,922, GRCh37; NM_015190, exon 3), later confirmed by Sanger sequencing. This aspartic acid is conserved among all species (MutationTaster2),[31] and the change to asparagine is predicted to be probably damaging, with a PolyPhen-2 score of 0.999. We confirmed segregation of this variant with disease in all 17 of the 06NZ-TRB1 family members analyzed (7 affected and 10 unaffected individuals). This variant was allocated the dbSNP identifier rs200630658 and was reported at a heterozygote (C/T) frequency of 0.002 in exome sequencing data from 662 individuals (The ClinSeq Project[42]). It is present twice in the Exome Aggregation Consortium database with an allele frequency of 1.65e-05.[41]

COL17A1 and *DNAJC9* Variant Screening in Additional Pedigrees

Members from 3 subsequently identified ERED families underwent genetic screening at *COL17A1* c.3156C→T and *DNAJC9*

Table 2. Candidate Heterozygous Variants at *COL17A1* and *DNAJC9* Observed in 2 Affected Individuals within the chr10: 12,576,562-112,763,135 Linkage Region by Exome Sequencing (Positive DNA Strand)

Gene Symbol	Gene Name	Chr10 Position (GRCh37)	Observed Allele	Reference Allele	Alteration Type	Coverage
COL17A1	*Collagen, type XVII, alpha 1*	105797446	A	G	Single base substitution in CDS; gain of splice donor site	27
DNAJC9	*DnaJ (Hsp40) homolog, subfamily C, member 9*	75005922	T	C	Nonsynonymous missense mutation causing substitution D112N; this amino acid is highly conserved in all species	33

c.334G→A, because segregation with disease status was confirmed in the 06NZ-TRB1 family at these 2 loci. A second affected family was identified in Tasmania, Australia (identifier, CDTAS1; Fig 1; Table 1). Clinically affected individuals in this pedigree showed recurrent ERED with a progressive increase in anterior stromal haze, similar to the 06NZ-TRB1 and UKOGA families (described above). The allelic status of 15 members of this family (10 affected and 5 unaffected individuals) for the *COL17A1* variant c.3156C→T (p.Gly1052Gly, chr10:105,797,446, GRCh37; ENST00000353479; NM_000494) and *DNAJC9* variant c.334G→A (p.D112N, chr10:75,005,922, GRCh37; NM_015190; Fig 1; Table 1) was determined with Sanger sequencing. All affected family members were heterozygous for the *COL17A1* variant (C/T), whereas unaffected family members were homozygous (C/C). However, at the *DNAJC9* variant c.334G→A, all individuals examined (10 affected and 5 unaffected) were homozygous for the wild-type c.334G allele. These results suggest that *COL17A1* is causative of disease in this family.

A third affected family was identified in Hamilton, New Zealand (identifier, 15NZ-LED1; Fig 1; Table 1). This family demonstrated clinical features consistent with ERED. Of the 4 family members tested, 3 were affected and 1 was considered typically too young, at 6 years of age, to demonstrate symptoms. All 4 family members tested were heterozygous for the aberrant *COL17A1* variant c.3156C→T. The *DNAJC9* variant c.334G→A was not present in the 15NZ-LED1 family. Our results suggest that the youngest family member, although currently asymptomatic, likely will demonstrate signs of the disease in the near future.

The fourth family with ERED was identified in the United Kingdom (identifier, UKOGA; Fig 1; Table 1). Analysis of the variant loci confirmed segregation of *COL17A1* c.3156C→T with disease (present in 7 affected members and absent in 2 unaffected members), but not *DNAJC9* c.334G→A, which was not present in any family members.

Microsatellite Screening across Epithelial Recurrent Erosion Dystrophy Families

Two microsatellite markers flanking the *COL17A1* c.3156C→T variant—*COL17A1* (20×AT) and *OBFC1* (19×CA), as shown in Supplemental Figure 1 (available at www.aaojournal.org)—indicate segregation of the haplotype *COL17A1* number 7 allele (C7; 7 repeats) and the *OBFC1* number 12 allele (012; 12 repeats) in affected individuals in all 4 families (provided in Supplemental Table 5, available at www.aaojournal.org). In the 06NZ-TRB1 family, 5 of 5 affected family members and 2 of 4 unaffected family members carry the C7/012 haplotype. All UKOGA family members tested carry the C7/012 haplotype (3 affected and 2 unaffected individuals), as with the 15NZ-LED1 family (3 affected individuals). In the CDTAS1 family, 9 of 9 affected family members carry the C7/012 haplotype, compared with only 1 of 4 unaffected family members.

Expression of COL17A1 and DNAJC9 in Human Corneal Tissue

Immunohistochemistry analysis was used to examine expression of COL17A1 and DNAJC9 in a fresh keratoconic cornea (Fig 4). COL17A1 is expressed in both corneal epithelial cells and the Bowman layer (basement membrane; Fig 4, red), whereas DNAJC9 is expressed in the Bowman layer of the corneal epithelium (Fig 4, green). The pattern of DNAJC9 localization is distinct from that of COL17A1.

Expression of *Col17a1* and Dnajc9 Proteins in Zebrafish

The Dnajc9 and Col17a1 staining in our adult (13 months after fertilization) zebrafish samples suggests protein presence in the external surface membranes of cells in the superficial squamous layer (Fig 5). In embryonic fish 3 days after fertilization, Dnajc9 and Col17a1 are present throughout the 2-cell layer of the developing cornea (Fig 5). Dnajc9 staining also appears to be present in the migrating endothelial cells, which at 3 days after fertilization are moving from the limbus to the cornea.[43] Both Col17a1 and Dnajc9 are expressed in different corneal layers in the adult zebrafish compared with human keratoconic tissue.

Expression of *C0117a1* and *Dnajc9* Transcripts in Zebrafish

At 50 hours after fertilization, the *Col17a1a* transcript is present in a punctate pattern on epithelial cells across the embryo, including the cornea (Fig 6). The *Col17a1b* transcript is expressed within neuromast cells, consistent with previous observations by Kim et al,[36] and is absent in the cornea.

At 50 hours after fertilization, *Dnajc9* is expressed throughout the head region of the embryo, including in the retinal proliferative zone, as described previously (Fig 6).[44] There is no clear evidence to support corneal expression of *Dnajc9* in embryos 50 hours after fertilization. However, under stress conditions induced by ethanol exposure, we observe upregulation of Dnacj9 in the head of embryos 2 days after fertilization, including the cornea, as shown in Supplemental Figure 5 (available at www.aaojournal.org).

Transient Knockdown of *Col17a1a* and *Dnajc9* with Morpholinos

We transiently knocked down *Col17a1a* using a translation-blocking morpholino. At 3 days after fertilization, we observed morphant embryos with atypical tail morphologic features, where the tip of the tail is distended compared with embryos injected with the standard morpholino control (Fig 7). Several morphants demonstrated heart edema and spinal curvature (Fig 7, arrow). No obvious changes were present in the morphant eye, although phenotypic characterization is limited by the sensitivity of this tissue to disruption during microdissection.

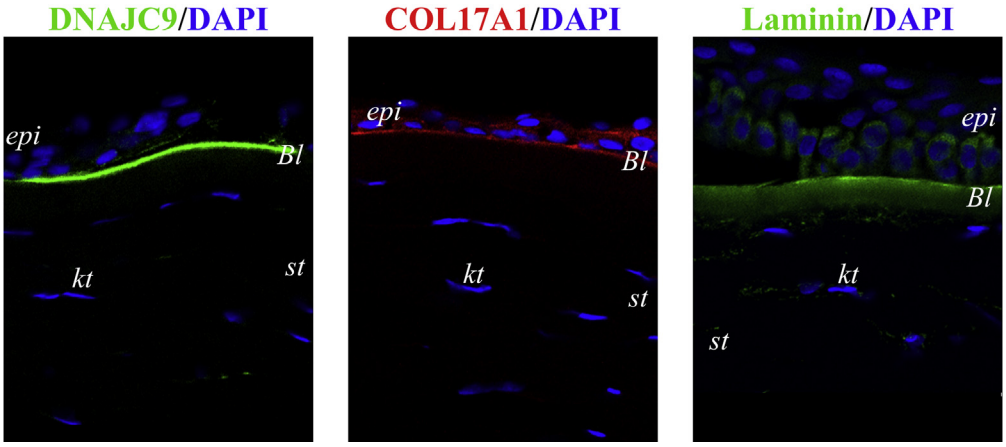

Figure 4. Localization of DNAJC9 (green), COL17A1 (red), and laminin (green) proteins in fresh human keratoconic cornea. DNAJC9 localizes to the Bowman layer (Bl). COL17A1 protein localizes to the Bowman layer and throughout the epithelial cells. Laminin marks the Bowman layer and adhering epithelial cells. epi = Epithelium; kt = keratocytes; st = stroma.

When we transiently knocked down *Dnajc9* with a splice-blocking morpholino, embryos 3 days after fertilization demonstrated a bent spine phenotype, which was not observed in control-injected morphants (Fig 7). No obvious ocular phenotype was observed in the *Dnajc9* morphants.

Discussion

In this study, we used genetic linkage to identify a haplotype on chr10:12,576,562−112,763,135 associated with autosomal dominant corneal ERED. Further characterization of the area with exome sequencing allowed us to show independently that the *COL17A1* genomic variant c.3156C→T segregates with affected individuals and is likely to be causative of disease in the 06NZ-TRB1 family. The presence of this same variant in a further 3 white ERED families (15NZ-LED1, CDTAS1, and UKOGA) suggests that it is highly likely to be the causative mutation and is prevalent in autosomal dominant ERED. Jonsson et al[13] recently identified a missense mutation in *COL17A1* (c.2816C→T, p.T939I) in a Northern Swedish family with ERED. A sequence variant in *COL17A1* (c.3156C→T) identified in the misclassified Thiel-Benhke dystrophy[12] was reported as a nonpathogenic synonymous variant[40]; however, Jonsson et al predicted that this variant leads to the introduction of a splice donor site and causes truncation of exon 46 (p.(Gly1052_Thr1070delinsAla)), and therefore is highly likely to be pathogenic. Combined with the findings in our 4 families described here, the c.3156C→T *COL17A1* variant is causative and *COL17A1* is an integral player in the pathogenesis of corneal ERED.

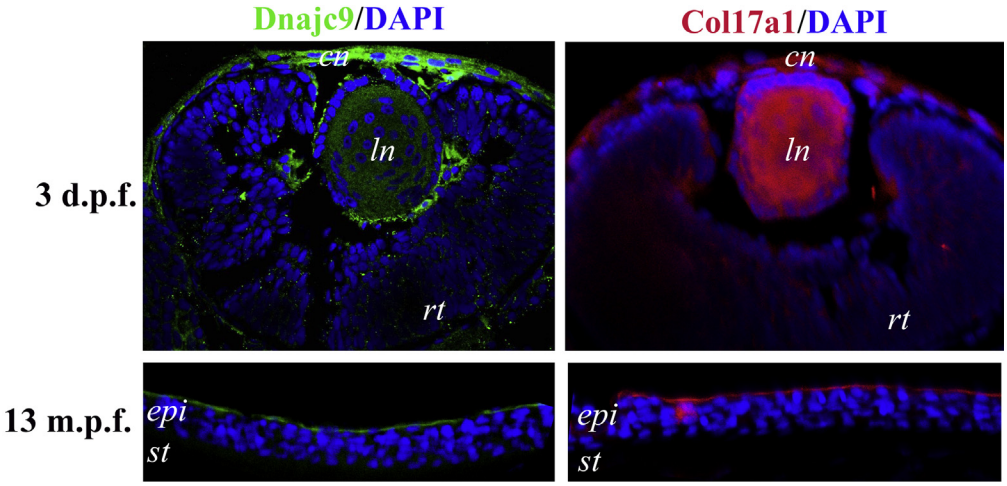

Figure 5. Immunohistochemistry staining results for Dnajc9 and Col17a1 protein in zebrafish cornea. Both Dnajc9 (green) and Col17a1 (red) proteins are present in the dual cell layers of the developing zebrafish cornea (3 days after fertilization [d.p.f.]). In the adult zebrafish cornea (13 months after fertilization [m.p.f.]), Dnajc9 and Col17a1 expression is restricted to the external surface membrane of the superficial epithelial cells. 4′,6-Diamidino-2-phenylindole staining (blue) indicates cell nuclei. cn = Cornea; epi = epithelium; ln = lens; rt = retina; st = stroma.

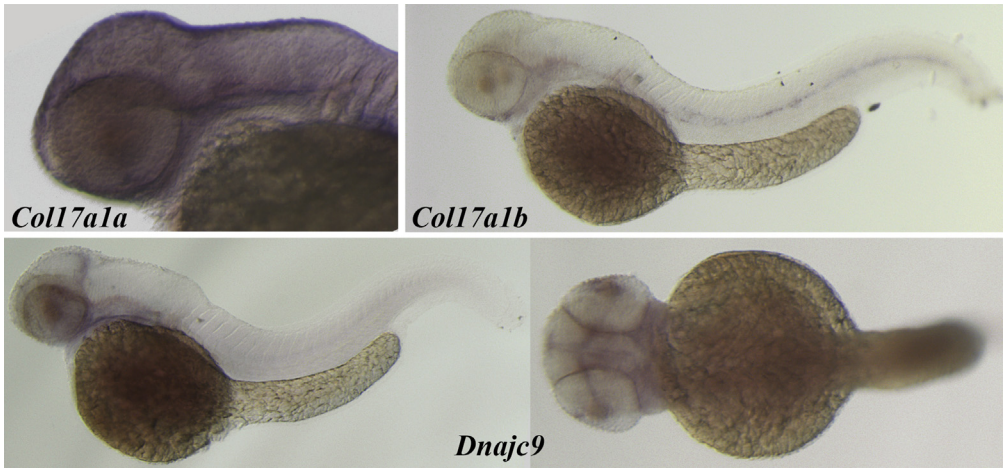

Figure 6. Photomicrographs obtained after whole-mount in situ hybridization was performed using antisense probes to the Col17a1a, Col17a1b, and *Dnajc9* genes on embryos 50 hours after fertilization and visualized with alkaline phosphatase–mediated staining. Col17a1a is observed in a punctate pattern on the epithelium, including over the developing cornea. Col17a1b transcripts are evident in the neuromast cells. Diffuse staining for *Dnajc9* transcript was observed in the head region and retinal proliferative zone of the zebrafish embryos (lateral and dorsal views shown).

In the index 06NZ-TRB1 New Zealand family, although numerous fine, small (25–100 μm), grey stromal flecks are present, it is the larger grey-white opacities at the level of the Bowman layer and immediately subjacent anterior stroma that distinguish the corneal phenotype from other corneal fleck dystrophies. Subtle corneal flecks are common yet asymptomatic and can be associated with contact lens wear, drugs, and inherited corneal dystrophies. Although on clinical biomicroscopy such flecks may appear to have a predominantly pre–Descemet membrane stromal location (e.g., Maeder Danos) or anterior stromal location (e.g., Francois Neetans), more typically, and especially on assessment by in vivo confocal microscopy, these flecks are variably distributed throughout the stroma.[45,46] Because these flecks typically are asymptomatic, there are few histologic data available, but they may represent enlarged or metabolically altered keratocytes or stromal deposits.[45–47]

In the index 06NZ-TRB1 New Zealand family, the small grey flecks are limited to the very anterior 20% of stroma (clinically and by IVCM) and extend from the central to peripheral cornea. But these flecks are not in isolation unique to, or diagnostic of, the corneal phenotype. However, the larger, focal grey-white, predominantly disk-shaped, circular, or wreath-like lesions (with central clarity), which vary from 0.2 to 1.5 mm in diameter, in conjunction with these aforementioned small, grey anterior stromal flecks, seem to be clinically diagnostic of this variant fleck and anterior membrane dystrophy (see Supplemental Fig 2, available at www.aaojournal.org). The larger grey-white lesions typically are few (range, 5–10). Prominent corneal nerves are present variably, but this is not a feature unique to this dystrophy.

Based on the available genealogic information, the 4 ERED families we have described are not knowingly related to each other. Our haplotype analysis with flanking microsatellite markers suggests that a C7/012 haplotype cosegregates with the c.3156C→T *COL17A1* variant in affected individuals. The discovery of this haplotype is consistent with a founder effect. Because the white population in Australia and New Zealand is derived largely from United Kingdom emigrants, it is possible that these families share a common ancestor.

There is biological evidence supporting an essential role of COL17A1 in the cornea. COL17A1, a member of the collagen family, is an integral part of the hemidesmosome structure. Our observed expression of COL17A1 in the corneal epithelium is consistent with its reported role as a hemidesmosome protein,[48,49] suggesting a function biologically relevant to the ERED phenotype. Furthermore, COL17A1 is associated with other diseases characterized by compromised epithelial attachment. Autoimmunity against COL17A1 produces the skin-blistering disease bullous pemphigoid,[50] whereas mutations in *COL17A1* cause the recessive, mechanically induced skin-blistering disease junctional epidermolysis bullosa,[51] which manifests as corneal erosion in many patients.[52] COL17A1 is linked to keratinocyte mobility,[53] and increased levels of COL17A1 have been observed during corneal wound healing,[54] suggesting it plays a crucial role not only in maintaining epithelial attachment, but also in recovering from injury.[53] Our expression analysis of human keratoconic corneal samples indicates that COL17A1 is present in the Bowman layer and around the epithelial cells, which is comparable with previous corneal findings.[13,55,56] Although our expression analysis was performed on keratoconic cornea, no difference in COL17A1 expression is found between keratoconic and normal corneal tissue.[13,56]

We identified a second potentially pathogenic variant in our original New Zealand family (06NZ-TRB1) in the *DNAJC9* gene (c.334G→A, p.D112N); this is the only variant identified in our exome sequencing data set (after filtering) that is a clear missense change. DNAJC9 is a member of the heat shock (HSP40) family of proteins and is purported to have a role in the molecular chaperoning of

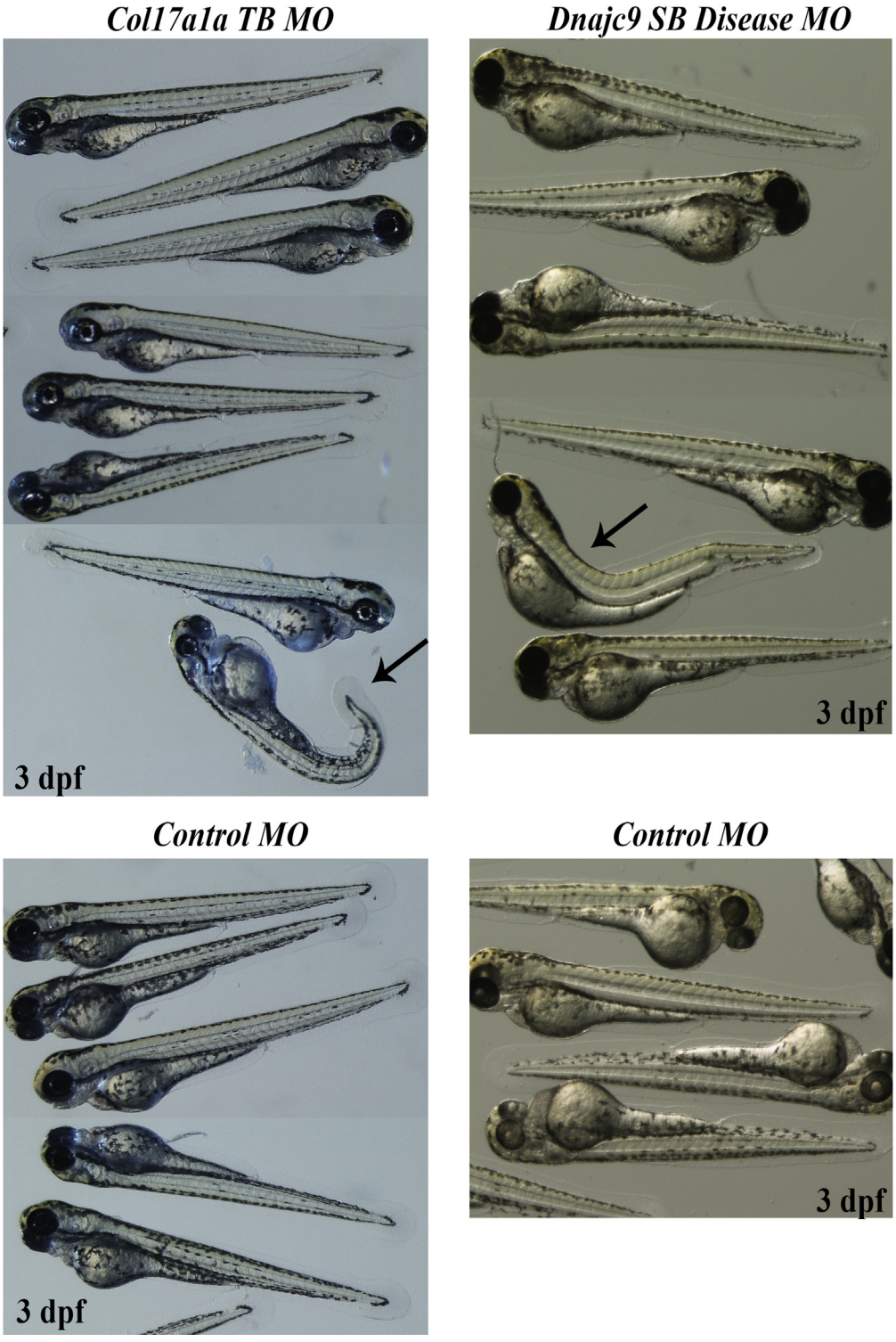

Figure 7. Photographs of zebrafish injected with 0.25 pmol *Col17a1* TB morpholino (MO), 0.5 pmol *Dnajc9* SB (disease exon) MO, or 0.5 pmol control MO obtained 3 days after fertilization (dpf). *Col17a1a* TB morphants present with morphologic changes in the shape of the tail tip and occasional heart edema (arrow). Although most *Dnajc9* SB (disease exon) morphants appear unaffected, several demonstrated spine curvature (arrow).

HSP70 family members. In human tissue, *DNAJC9* is expressed ubiquitously and is upregulated in response to stress.[57] Because the nonsynonymous *DNAJC9* variant is found in only 1 of the 4 ERED families (06NZ-TRB1), we conclude that it is not necessary for ERED corneal disease, but it cannot be excluded as a modifier of disease severity. Of note, disease presentation in the 06NZ-TRB1 family trended toward an earlier age at onset than in the

additional 3 families (Table 1). DNAJC9 expression has not been characterized previously in the human cornea. The expression pattern within the human keratoconic cornea is consistent with a potential role in corneal adhesion. Colocalization of DNAJC9 and COL17A1 in both human and zebrafish cornea is suggestive of a potential interaction between the 2 proteins, possibly with regard to response to injury and tissue regeneration. We hypothesize that under stress conditions, such as mild trauma, mutant DNAJC9 protein may not adequately perform its roles in regulating cell proliferation, survival, and apoptosis by chaperoning HSP70s.

In addition, we examined the expression pattern of *COL17A1* and *DNAJC9* orthologs (protein and transcript) in the zebrafish. The zebrafish cornea contains all 5 of the major corneal layers (including the Bowman layer) and is readily visible early in development.[43] The mature zebrafish corneal epithelium is 4 to 6 cells deep, constituting approximately 60% of the corneal thickness, whereas the stroma comprises a further 30%.[43] Although we did observe Col17a1 and Dnajc9 in the zebrafish cornea, these proteins appeared to be localized to the squamous epithelial cells on the surface of the cornea. The difference in protein localization between the zebrafish and human corneas may be attributed to the differences in cornea between these 2 species; the zebrafish cornea presumably is under less mechanical stress than the human cornea (absence of eyelids in the fish). Therefore, zebrafish epithelial cells may not require the same tight anchoring to the Bowman layer. The zebrafish has undergone historical genome duplication,[58] resulting in 2 copies of many genes, some of which have undergone functional divergence. Whole-mount in situ hybridization analysis of gene expression was used to identify the zebrafish corneal ortholog of human *COL17A1* in zebrafish embryos. The expression of the *COL17A1* homologs has been assessed previously in zebrafish with regard to junctional epidermolysis bullosa mutations.[36] We confirmed the previously published expression patterns of the zebrafish orthologs of *COL17A1:Col17a1a* and *Col17a1b*,[36,44] and established that *Col17a1a* is likely to be the functional ortholog in zebrafish cornea. We did not observe high expression of *Dnajc9* in embryos; however, as a member of the heat shock protein family, high expression is not necessarily expected from embryos in the absence of stress. Under stress conditions induced by ethanol exposure,[59] we noted increased Dnajc9 expression in the zebrafish cornea. When *Col17a1a* was knocked down transiently during early development, we observed changes to tail morphologic features, but no obvious alteration to the gross corneal or ocular phenotype. A similar tail distension phenotype was characterized by Kim et al,[36] who identified the phenotype as resulting from vacuolization in the epidermis and attributed it to compromised hemidesmosomes. Transient knockdown of *Dnajc9* caused spinal curvature in some morphants. Accurate characterization of the cornea of the developing zebrafish is challenging because morphologic artefacts are introduced readily during the microdissection process. As a further limitation, the zebrafish cornea is not developed fully until adulthood,[43] challenging the feasibility of transient, morpholino-induced gene knockdowns.

Until recently, morpholinos were considered the gold standard approach; however, phenotypic discrepancies now are known to be common between morphant and knockout zebrafish.[60] The CRISPR/Cas9 genome-editing technique opens up exciting opportunities to introduce (via homology-directed repair) our identified *COL17A1* and *DNAJC9* variants into zebrafish,[61] establishing lines suitable for examining the role of these genes in adult zebrafish cornea using both ophthalmic (e.g., optical coherence tomography[62]) and molecular diagnostic tools. We have found that although the zebrafish is an ideal model for genetic engineering of the *Col17a1a* variant c.3156C→T, it has limitations for use in examining corneal dystrophy onset during early development.

The rare *COL17A1* disease-causing variant (c.3156C→T) occurring in our 4 families with phenotypically similar disease replicates the association of a *COL17A1* missense mutation (c.2816C→T) in the Swedish ERED family.[13] It also suggests that the phenotype described as Thiel-Behnke by Yee et al[12] is the result of the same *COL17A1* disease-causing variant detected in our families. This study expands the phenotypic spectrum of *COL17A1* disease from autosomal recessive epidermolysis bullosa to autosomal dominant ERED and suggests that COL17A1 is a key protein in maintaining corneal epithelium integrity.

Acknowledgments. The authors thank all the family members for their participation in this study, Alhad Mahagaonkar for managing the zebrafish facility at The University of Auckland, the staff at the Otago Genomics Facility for processing the exome sequencing samples, and the Exome Aggregation Consortium and other groups for providing exome variant data for comparison. A full list of contributing groups can be found at http://exac.broadinstitute.org/about.

References

1. Weiss JS, Moller HU, Aldave AJ, et al. IC3D classification of corneal dystrophies—edition 2. Cornea 2015;34:117–59.
2. Weiss JS, Moller HU, Lisch W, et al. The IC3D classification of the corneal dystrophies. Cornea 2008;27(Suppl 2): S1–83.
3. Vincent AL, Markie DM, De Karolyi B, et al. Exclusion of known corneal dystrophy genes in an autosomal dominant pedigree of a unique anterior membrane corneal dystrophy. Mol Vis 2009;15:1700–8.
4. Vincent AL. Corneal dystrophies and genetics in the International Committee for Classification of Corneal Dystrophies era: a review. Clin Experiment Ophthalmol 2014;42:4–12.
5. Munier FL, Frueh BE, Othenin-Girard P, et al. BIGH3 mutation spectrum in corneal dystrophies. Invest Ophthalmol Vis Sci 2002;43:949–54.
6. Li S, Tiab L, Jiao X, et al. Mutations in PIP5K3 are associated with Francois-Neetens mouchetee fleck corneal dystrophy. Am J Hum Genet 2005;77:54–63.
7. Franceschetti A, Klein D. Cornea. In: Waardenburg PJ, Franceschetti A, Klein D, eds. Genetics and Ophthalmology. Springfield, IL: Charles C. Thomas; 1961.

8. Franceschetti A. Hereditaere rezidivierende Erosion der Hornhaut. Z Augenheilk 1928;66:309–16.
9. Lisch W, Bron AJ, Munier FL, et al. Franceschetti hereditary recurrent corneal erosion. Am J Ophthalmol 2012;153:1073–1081.e4.
10. Lisch W, Kivela T. Individual phenotypic variances in a family with Thiel-Behnke corneal dystrophy. Cornea 2013;32:e192–3.
11. Nakamura H, Li FT, Foltermann MO, et al. Individual phenotypic variances in a family with Thiel-Behnke corneal dystrophy. Cornea 2012;31:1217–22.
12. Yee RW, Sullivan LS, Lai HT, et al. Linkage mapping of Thiel-Behnke corneal dystrophy (CDB2) to chromosome 10q23-q24. Genomics 1997;46:152–4.
13. Jonsson F, Bystrom B, Davidson AE, et al. Mutations in Collagen, type XVII, Alpha 1 (*COL17A*) cause epithelial recurrent erosion dystrophy (ERED). Hum Mutat 2015;36:463–73.
14. Eckard A, Stave J, Guthoff RF. In vivo investigations of the corneal epithelium with the confocal Rostock Laser Scanning Microscope (RLSM). Cornea 2006;25:127–31.
15. Steger B, Speicher L, Philipp W, Bechrakis NE. In vivo confocal microscopic characterisation of the cornea in chronic graft-versus-host disease related severe dry eye disease. Br J Ophthalmol 2015;99:160–5.
16. Ruschendorf F, Nurnberg P. ALOHOMORA: a tool for linkage analysis using 10K SNP array data. Bioinformatics 2005;21:2123–5.
17. O'Connell JR, Weeks DE. PedCheck: a program for identification of genotype incompatibilities in linkage analysis. Am J Hum Genet 1998;63:259–66.
18. Abecasis GR, Cherny SS, Cookson WO, Cardon LR. Merlin—rapid analysis of dense genetic maps using sparse gene flow trees. Nat Genet 2002;30:97–101.
19. Gudbjartsson DF, Thorvaldsson T, Kong A, et al. Allegro version 2. Nat Genet 2005;37:1015–6.
20. Kong A, Thorleifsson G, Gudbjartsson DF, et al. Fine-scale recombination rate differences between sexes, populations and individuals. Nature 2010;467:1099–103.
21. Jensen LJ, Kuhn M, Stark M, et al. STRING 8—a global view on proteins and their functional interactions in 630 organisms. Nucleic Acids Res 2009;37(Database issue):D412–6.
22. Vincent AL, Jordan CA, Cadzow MJ, et al. Mutations in the zinc finger protein gene, *ZNF469*, contribute to the pathogenesis of keratoconus. Invest Ophthalmol Vis Sci 2014;55:5629–35.
23. Li H, Durbin R. Fast and accurate long-read alignment with Burrows-Wheeler transform. Bioinformatics 2010;26:589–95.
24. Broad Institute. Picard. Cambridge, MA: Broad Institute; 2012. Available at: http://broadinstitute.github.io/picard/. Accessed December 2013.
25. McKenna A, Hanna M, Banks E, et al. The Genome Analysis Toolkit: a MapReduce framework for analyzing next-generation DNA sequencing data. Genome Res 2010;20:1297–303.
26. DePristo MA, Banks E, Poplin R, et al. A framework for variation discovery and genotyping using next-generation DNA sequencing data. Nat Genet 2011;43:491–8.
27. Cingolani P, Platts A, Wang le L, et al. A program for annotating and predicting the effects of single nucleotide polymorphisms, SnpEff: SNPs in the genome of *Drosophila melanogaster* strain w1118; iso-2; iso-3. Fly (Austin) 2012;6:80–92.
28. National Heart, Lung, and Blood Institute. NHLBI GO Exome Sequencing Project. Exome Variant Server. 2014. Available at: http://evs.gs.washington.edu/EVS/. Accessed December 2, 2014.
29. Genomes Project C, Abecasis GR, Altshuler D, et al. A map of human genome variation from population-scale sequencing. Nature 2010;467:1061–73.
30. Schwarz JM, Rodelsperger C, Schuelke M, Seelow D. MutationTaster evaluates disease-causing potential of sequence alterations. Nat Methods 2010;7:575–6.
31. Schwarz JM, Cooper DN, Schuelke M, Seelow D. MutationTaster2: mutation prediction for the deep-sequencing age. Nat Methods 2014;11:361–2.
32. Desmet FO, Hamroun D, Lalande M, et al. Human Splicing Finder: an online bioinformatics tool to predict splicing signals. Nucleic Acids Res 2009;37:e67.
33. Adzhubei IA, Schmidt S, Peshkin L, et al. A method and server for predicting damaging missense mutations. Nat Methods 2010;7:248–9.
34. Kurpakus MA, Daneshvar C, Davenport J, Kim A. Human corneal epithelial cell adhesion to laminins. Curr Eye Res 1999;19:106–14.
35. Thisse C, Thisse B. High-resolution in situ hybridization to whole-mount zebrafish embryos. Nat Protoc 2008;3:59–69.
36. Kim SH, Choi HY, So JH, et al. Zebrafish type XVII collagen: gene structures, expression profiles, and morpholino "knockdown" phenotypes. Matrix Biol 2010;29:629–37.
37. Wales HJ. A family history of corneal erosions. Trans Ophthalmol Soc N Z 1955;8:77–8.
38. Kobayashi A, Yokogawa H, Sugiyama K. In vivo laser confocal microscopy of Bowman's layer of the cornea. Ophthalmology 2006;113:2203–8.
39. Genomes Project C, Abecasis GR, Auton A, et al. An integrated map of genetic variation from 1,092 human genomes. Nature 2012;491:56–65.
40. Sullivan LS, Zhao X, Bowne SJ, et al. Exclusion of the human collagen type XVII (*COL17A1*) gene as the cause of Thiel-Behnke corneal dystrophy (CDB2) on chromosome 10q23-q25. Curr Eye Res 2003;27:223–6.
41. Broad Institute. Exome Aggregation Consortium (ExAC). 2015. Available at: http://exac.broadinstitute.org/. Accessed June 2015.
42. Biesecker LG, Mullikin JC, Facio FM, et al. The ClinSeq Project: piloting large-scale genome sequencing for research in genomic medicine. Genome Res 2009;19:1665–74.
43. Zhao XC, Yee RW, Norcom E, et al. The zebrafish cornea: structure and development. Invest Ophthalmol Vis Sci 2006;47:4341–8.
44. Thisse B, Thisse C. Fast Release Clones: A High Throughput Expression Analysis. ZFIN Direct Data Submission, 2004. Available at: https://zfin.org/ZDB-PUB-040907-1. Accessed June 4, 2015.
45. Grupcheva CN, Malik TY, Craig JP, et al. Microstructural assessment of rare corneal dystrophies using real-time in vivo confocal microscopy. Clin Experiment Ophthalmol 2001;29:281–5.
46. Klintworth GK. Corneal dystrophies. Orphanet J Rare Dis 2009;23:7. http://dx.doi.org/10.1186/1750-1172-4-7.
47. Vincent AL, Patel DV, McGhee CN. Inherited corneal disease: the evolving molecular, genetic and imaging revolution. Clin Experiment Ophthalmol 2005;33:303–16.
48. Hopkinson SB, Baker SE, Jones JC. Molecular genetic studies of a human epidermal autoantigen (the 180-kD bullous pemphigoid antigen/BP180): identification of functionally important sequences within the BP180 molecule and evidence for an interaction between BP180 and alpha 6 integrin. J Cell Biol 1995;130:117–25.
49. Koster J, Geerts D, Favre B, et al. Analysis of the interactions between BP180, BP230, plectin and the integrin alpha6beta4

important for hemidesmosome assembly. J Cell Sci 2003;116(Pt 2):387–99.
50. Olasz EB, Yancey KB. Bullous pemphigoid and related subepidermal autoimmune blistering diseases. Curr Dir Autoimmun 2008;10:141–66.
51. Bruckner-Tuderman L, Has C. Molecular heterogeneity of blistering disorders: the paradigm of epidermolysis bullosa. J Invest Dermatol 2012;132(E1):E2–5.
52. Fine JD, Johnson LB, Weiner M, et al. Eye involvement in inherited epidermolysis bullosa: experience of the National Epidermolysis Bullosa Registry. Am J Ophthalmol 2004;138:254–62.
53. Loffek S, Hurskainen T, Jackow J, et al. Transmembrane collagen XVII modulates integrin dependent keratinocyte migration via PI3K/Rac1 signaling. PLoS One 2014;9.e87263:1−11.
54. Gipson IK, Spurr-Michaud S, Tisdale A, Keough M. Reassembly of the anchoring structures of the corneal epithelium during wound repair in the rabbit. Invest Ophthalmol Vis Sci 1989;30:425–34.
55. Anhalt GJ, Jampel HD, Patel HP, et al. Bullous pemphigoid autoantibodies are markers of corneal epithelial hemidesmosomes. Invest Ophthalmol Vis Sci 1987;28:903–7.
56. Cheng EL, Maruyama I, SundarRaj N, et al. Expression of type XII collagen and hemidesmosome-associated proteins in keratoconus corneas. Curr Eye Res 2001;22:333–40.
57. Han C, Chen T, Li N, et al. HDJC9, a novel human type C DnaJ/HSP40 member interacts with and cochaperones HSP70 through the J domain. Biochem Biophys Res Commun 2007;353:280–5.
58. Postlethwait JH, Woods IG, Ngo-Hazelett P, et al. Zebrafish comparative genomics and the origins of vertebrate chromosomes. Genome Res 2000;10:1890–902.
59. Kashyap B, Pegorsch L, Frey RA, et al. Eye-specific gene expression following embryonic ethanol exposure in zebrafish: roles for heat shock factor 1. Reprod Toxicol 2014;43:111–24.
60. Schulte-Merker S, Stainier DY. Out with the old, in with the new: reassessing morpholino knockdowns in light of genome editing technology. Development 2014;141:3103–4.
61. Irion U, Krauss J, Nusslein-Volhard C. Precise and efficient genome editing in zebrafish using the CRISPR/Cas9 system. Development 2014;141:4827–30.
62. Rao KD, Verma Y, Patel HS, Gupta PK. Non-invasive ophthalmic imaging of adult zebrafish eye using optical coherence tomography. Curr Sci 2006;90:1506–10.

Footnotes and Financial Disclosures

Originally received: August 20, 2015.
Final revision: November 6, 2015.
Accepted: December 5, 2015.
Available online: January 16, 2016. Manuscript no. 2015-1436.

[1] Department of Ophthalmology, New Zealand National Eye Centre, Faculty of Medical and Health Sciences, The University of Auckland, Auckland, New Zealand.

[2] Department of Biochemistry, Dunedin School of Medicine, Otago University, Dunedin, New Zealand.

[3] Department of Corneal and External Eye Diseases, St. Paul's Eye Unit, Royal Liverpool University Hospital, Liverpool, United Kingdom.

[4] Pathology Department, Dunedin School of Medicine, Otago University, Dunedin, New Zealand.

[5] Menzies Institute for Medical Research, University of Tasmania, Hobart, Australia.

[6] Lions Eye Institute, University of Western Australia, Perth, Australia.

[7] Department of Eye and Vision Science, Institute of Ageing and Chronic Disease, University of Liverpool, Liverpool, United Kingdom.

[8] Department of Molecular Medicine and Pathology, Faculty of Medical and Health Sciences, The University of Auckland, Auckland, New Zealand.

[9] Eye Department, Greenlane Clinical Centre, Auckland District Health Board, Auckland, New Zealand.

Presented as a poster at: Association for Research in Vision and Ophthalmology Annual Meeting, Denver, Colorado, May 2015.

Financial Disclosure(s):
The author(s) have no proprietary or commercial interest in any materials discussed in this article.

Supported by the Auckland Medical Research Foundation, Auckland, New Zealand; the Maurice and Phyllis Paykel Trust, Auckland, New Zealand; The University of Auckland School of Medicine Foundation Grant, Auckland, New Zealand; The University of Auckland School of Medicine PBRF Grant, Auckland, New Zealand; the Save Sight Society New Zealand, Auckland, New Zealand; National Health and Medical Research Council, Canberra, Australia (grant no.: 1023911); and Northern Ireland Research and Development Office RRG grant, Belfast, United Kingdom.

Author Contributions:

Conception and design: Oliver, van Bysterveldt, Markie, Sherwin, Crosier, McGhee, Vincent

Analysis and interpretation: Oliver, van Bysterveldt, Cadzow, Markie, Hewitt, Mackey, Willoughby, Sherwin, Crosier, McGhee, Vincent

Data collection: Oliver, van Bysterveldt, Steger, Romano, Markie, Hewitt, Mackey, Willoughby, Vincent

Obtained funding: none

Overall responsibility: Oliver, van Bysterveldt, Cadzow, Steger, Romano, Markie, Hewitt, Mackey, Willoughby, Sherwin, Crosier, McGhee, Vincent

Abbreviations and Acronyms:
ERED = epithelial recurrent erosion dystrophy; **IVCM** = in vivo confocal microscopy; **PBS** = phosphate-buffered saline; **PCR** = polymerase chain reaction.

Correspondence:
Andrea L. Vincent, MD, FRANZCO Department of Ophthalmology, New Zealand National Eye Centre, Faculty of Medical and Health Sciences, The University of Auckland, Private Bag 92019, Victoria St West, Auckland, 1142 New Zealand. E-mail: a.vincent@auckland.ac.nz.